


Cite this: *RSC Adv.*, 2020, 10, 28180

Received 1st June 2020

Accepted 17th July 2020

DOI: 10.1039/d0ra04812g

rsc.li/rsc-advances

# Modulator-free approach towards missing-cluster defect formation in Zr-based UiO-66†

Patchanee Chammingkwan,<sup>a</sup> Goji Yildun Shangum,<sup>ab</sup> Le Thi Tuyet Mai,<sup>a</sup> Priyank Mohan,<sup>a</sup> Ashutosh Thakur,<sup>a</sup> Toru Wada<sup>a</sup> and Toshiaki Taniike<sup>\*a</sup>

By rigorous control of water, missing-cluster defects in Zr-based UiO-66 were generated to a remarkable extent without the need of acidic modulators. The presence of missing-cluster defects created hierarchical pore structures, which had a profound effect on the catalytic performance.

## Introduction

Metal-organic frameworks (MOFs), constructed by three-dimensional assembly of metal ions/metal clusters and organic ligands, represent an emerging class of porous materials. The high degree of structural tunability, well-defined and controllable porosity, high surface areas, and high concentration of isolated metal ions have made MOFs promising materials in various fields such as photocatalysis, catalysis, separation and purification, gas/energy storage, and sensing.<sup>1–5</sup> Recently, incorporation of defects in MOFs has attracted paramount attention. Removal of linkers widens a window for enhanced gas storage capacity and mass transportation.<sup>6–10</sup> Meanwhile, the left under-coordinated metal atoms serve as catalytically active sites, otherwise as anchoring sites for other active elements.<sup>11–13</sup> Here, the judicious control of defect formation is essential in achieving desired properties while maintaining well-defined and highly tunable structural features of the parent framework.

Among a known variety of MOFs, defect engineering has been extensively investigated for Zr-based UiO-66,<sup>6–32</sup> which is constructed by six-centred zirconium oxyhydroxide clusters linked *via* terephthalate linkers to form an **fcu** framework. In addition to its flexibility to tailor the functionality by the selection of the linker,<sup>18,19</sup> the high degree of connectivity between metal clusters and linkers permits the formation of defects at a high concentration without the collapse of the overall structure.<sup>6,20–23</sup> Two types of defects, missing-linker defects and missing-cluster defects, are known. The former is related to the irregular removal of linkers to

generate point defects; the latter is created by the coupled removal of metal clusters and linkers connected to them in a concentrated manner to form a nano-domain of the **reO** topology. Though these two types of defects are likely similar in terms of chemical nature, they can significantly impact the mechanical and physical properties.<sup>24</sup> Especially, the removal of clusters leaves meso-scale cavities to provide more open hierarchical pore structures that are beneficial for mass and proton transportation.<sup>25,26</sup>

Control over the missing-linker defect formation has been predominantly achieved through the addition of modulators.<sup>6–11,21,22,26,27</sup> It is widely accepted that monocarboxylic acid with a lower  $pK_a$  value than the original linker competitively coordinates with a metal cluster to facilitate the growth of crystals having a lower coordination number. On the other hand, limited modulators can promote the formation of the missing-cluster defects unless an excessive concentration is used.<sup>21</sup> Based on energetic preference in DFT calculations, it was reported that capping species dominates the defect formation (*i.e.* type and concentration) through steric repulsion and hydrogen bonding patterns.<sup>28</sup> So far, highly acidic modulators, particularly fluorinated carboxylic acids, were found to promote the formation of missing-cluster defects at a relatively small addition.<sup>21</sup> However, the persistent aspect of fluorinated organic molecules in the environment raises a challenge in practical applications. A new approach to incorporate and manipulate the missing-cluster defects in a simple and more environmentally friendly fashion is highly desired. Herein, we report a novel modulator-free approach where missing-cluster defects can be generated and manipulated to a remarkable extent only by controlling “water” as one of the synthetic constituents without the need of acidic modulators. It was also proven that the missing-cluster defects produced based on the said method is effective for catalysis.

## Experiment

### Synthesis of UiO-66

A series of UiO-66 samples was prepared according to the previously reported procedure.<sup>29</sup> 1.63 mmol of  $ZrCl_4$  in 30 mL of

<sup>a</sup>Graduate School of Advanced Science and Technology, Japan Advanced Institute of Science and Technology, 1-1 Asahidai, Nomi, Ishikawa 923-1292, Japan. E-mail: taniike@jaist.ac.jp

<sup>b</sup>Department of Chemistry, Faculty of Natural Sciences, University of Jos, P.M.B 2084, Jos Plateau State, Nigeria

† Electronic supplementary information (ESI) available: X-ray diffraction, transmission electron microscopy, thermogravimetric analysis,  $N_2$  adsorption/desorption measurement, X-ray photoelectron spectroscopy, acid-base titration, Fourier-transform infrared spectroscopy, analysis of reaction products, catalyst recyclability and structural retention. See DOI: 10.1039/d0ra04812g



dimethylformamide (DMF) and 2.28 mmol of terephthalic acid in 30 mL of DMF were mixed under N<sub>2</sub> atmosphere. A specified amount of deionized water (0.2, 0.4, 0.8, 1.2 and 2.0 mL, corresponding to the molar ratio of 7, 14, 27, 41 and 68 with respect to ZrCl<sub>4</sub>, respectively) was added to the solution mixture prior to heating at 100 °C for 12 h under stirring. The solid product was collected by centrifugation, repetitively washed with DMF and methanol, and finally dried under vacuum at 90 °C for 24 h. The samples were named as UiO-*X*, in which *X* indicates the volume of added water. UiO-66-CH<sub>3</sub> and UiO-66-NH<sub>2</sub> samples (denoted as UiO-CH<sub>3</sub>-*X* and UiO-NH<sub>2</sub>-*X*, respectively) were prepared using the same procedure, except 2-methylterephthalic acid or 2-aminoterephthalic acid was used instead of terephthalic acid.

## Results and discussion

In this work, water was used to control the defect formation in UiO-66. A small amount of water was added to the mixture strictly under N<sub>2</sub> to prevent water intrusion from the atmosphere due to the hygroscopic nature of ZrCl<sub>4</sub>. In the absence of water, only a trace amount of the solid product was formed, which is not unexpected as water is a requisite for the formation of the Zr<sup>4+</sup> oxo/peroxo cluster.<sup>30</sup> The addition of 0.2 mL of water (UiO-0.2) resulted in the formation of a white solid at a yield less than 50%, while the addition of water in the range of 0.4–2.0 mL (UiO-0.4, UiO-0.8, UiO-1.2 and UiO-2.0) led to similar product yields more than 80%. As the ZrCl<sub>4</sub> : H<sub>2</sub>O molar ratio of 1 : 8 is theoretically required for the formation of Zr<sub>6</sub>(OH)<sub>4</sub>O<sub>4</sub>(bdc)<sub>6</sub>, the low yield for UiO-0.2 was originated from an insufficient amount of water with respect to ZrCl<sub>4</sub>. The X-ray diffraction (XRD) patterns of all the samples exhibited the face-centered cubic lattice typical for the UiO-66 crystal (Fig. 1a and S1†). The crystallite size that was derived from the (111) reflection monotonously decreased by increasing the water amount, in agreement with the transmission electron microscopy observation (Fig. S4 and S7†). The reduction of the crystallite size was ascribed to accelerated

nucleation of the oxoclusters by water, thus changing the crystallization process from nucleation-limited to growth-limited crystallization.<sup>27,30</sup> From the XRD profiles, the broad diffraction peaks at  $2\theta = 5.9^\circ$ ,  $9.6^\circ$  and  $10.6^\circ$  were additionally observed for UiO-0.2, UiO-0.4 and UiO-0.8. These diffractions were similar to those reported by Goodwin and co-workers, when monocarboxylic acid was introduced as a modulator. They were assigned to the (110), (210) and (211) reflections of the **reo** topology.<sup>22</sup> The **reo** phase existed as a nano-domain where the cluster is eight-connected instead of twelve to generate an octahedral cavity, so called a missing-cluster defect. In the case of UiO-1.2, only the peak at  $5.9^\circ$  was found in addition to a typical diffraction of UiO-66. Though this peak is very broad with a diffuse feature, it is sufficiently distinguishable from the base line and can be assigned to the (110) reflection of the **reo** phase with the domain size even smaller than the other three samples. The same approach was extended to UiO-66-CH<sub>3</sub> and UiO-66-NH<sub>2</sub> using water in the range of 0.3–0.9 mL. In XRD, they possess an isostructure to that of UiO-66 (Fig. 1b, c, S2 and S3†). The appearance of the diffraction peak at  $2\theta = 5.9^\circ$  clearly evidenced the formation of the **reo** topology, emphasizing a crucial role of water on the formation of the missing-cluster defects regardless the type of the ligand. A similar tendency for the particle size reduction with the increase in the water amount was observed for both of the UiO-66-CH<sub>3</sub> and UiO-66-NH<sub>2</sub> series (Fig. S5–S7†). Among the employed linkers, UiO-66-NH<sub>2</sub> exhibited the smallest particle size at the same water amount due to the crystallization acceleration effect of the amino group.<sup>31</sup>

Based on the weight loss in the thermogravimetric (TG) analysis (Fig. S8 and Table S1†), all of the samples exhibited the number of the linker per cluster lower than 12. It must be noted that the TG method is known to be less accurate for the quantitative analysis of the organic content,<sup>12</sup> especially for the amino-substituted UiO-66-NH<sub>2</sub> that did not exhibit a clear plateau. However, the linker deficiency tended to be more pronounced for a smaller water amount for all the series. The

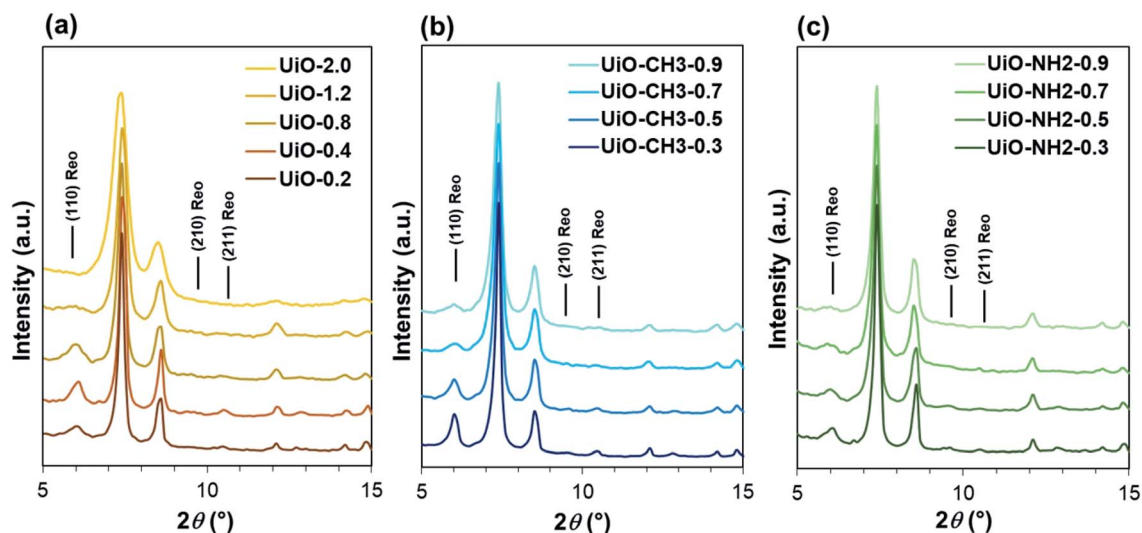


Fig. 1 XRD patterns of (a) UiO-66, (b) UiO-66-CH<sub>3</sub> and (c) UiO-66-NH<sub>2</sub> samples.

microporous surface area and the mesoporous surface area were acquired from  $N_2$  adsorption/desorption experiments. In Table S2,<sup>†</sup> the microporous surface area of UiO-66 samples decreased with the increase in the water amount, while the tendency was opposite for the mesoporous surface area. The increase in the mesoporous surface area is originated from the reduction of the particle size, in which the intergrown morphology created the interparticle channel having the size in the mesopore region. As a result, the differences in microporous and mesoporous surface areas among the samples are hardly explained by the presence of defects due to the strong influences of the particle size. Internal pore structures in relation to the type of defects were interpreted from the  $N_2$  adsorption/desorption isotherms (Fig. S9–S21<sup>†</sup>). The pore size distributions constructed by the NLDFT method for UiO-2.0 and UiO-1.2 exhibited a broad peak with a small shoulder (Fig. 2a). The peak top is positioned at 10 Å, slightly larger than the pore size typically reported for defect-free UiO-66.<sup>11,32</sup> Such an enlarged pore size has been reported for UiO-66 with a missing-linker defect where the shortage of the linkers from the metal cluster expanded the entire framework.<sup>6,11,12,32</sup> On the other hand, the rest of the samples including UiO-66-CH<sub>3</sub> and UiO-66-NH<sub>2</sub> series equipped two modes of pores (Fig. 2b and c). The first mode centred at 10 Å similar to those of UiO-2.0 and UiO-1.2, while the second mode appeared at 16 Å. The appearance of the second mode was associated with the removal of the cluster to generate an octahedral cavity.<sup>22,32</sup> These results agreed well with the observation of the **reo** topology by X-ray. Based on all the above observations, it was concluded that both of the missing-linker and missing-cluster defects co-existed in the samples, except UiO-2.0 that mainly contained the missing-linker defects. In the absence of modulators, the coordination vacancies can be filled by  $OH^-/H_2O$  and  $Cl^-$  (generated *in situ* from the hydrolysis of  $ZrCl_4$ ). X-ray photoelectron spectroscopy analysis (Fig. S22<sup>†</sup>) showed the absence of Cl, excluding  $Cl^-$  as the compensating group. Indeed, the acid–base titration of UiO-

66 revealed three reflection points (Fig. S23<sup>†</sup>), which are respectively attributed to  $\mu_3-OH$ ,  $Zr-OH_2$  and  $Zr-OH$ .<sup>33</sup> The latter two protons confirmed the charge compensation at the defective nodes by  $OH^-/H_2O$ .

In order to acquire the quantitative trend of the missing-cluster defect formation, the relative intensity of the (110) **reo** peak was calculated according to Shearer *et al.*<sup>21</sup> As depicted in Fig. 3, the relative intensity of the (110) **reo** peak decreased along with the increase in the water amount, except UiO-0.2. To date, the mechanism for the formation of the **reo** phase in UiO-66 has not been well understood. As a modulator is not present, the coordination equilibrium shift due to competitive coordination can be ruled out. Recently, the partially deprotonated ligand model was proposed.<sup>32</sup> In this model, the missing-cluster defects occur when ligands on the surface of adjacent clusters are partially deprotonated, thus being unable to accept the metal cluster between them. Herein, we did not observe the

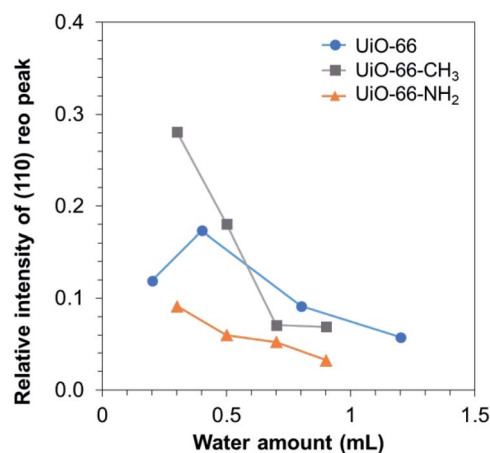


Fig. 3 Relative intensity of (110) **reo** peak for UiO-66, UiO-66-CH<sub>3</sub> and UiO-66-NH<sub>2</sub>.

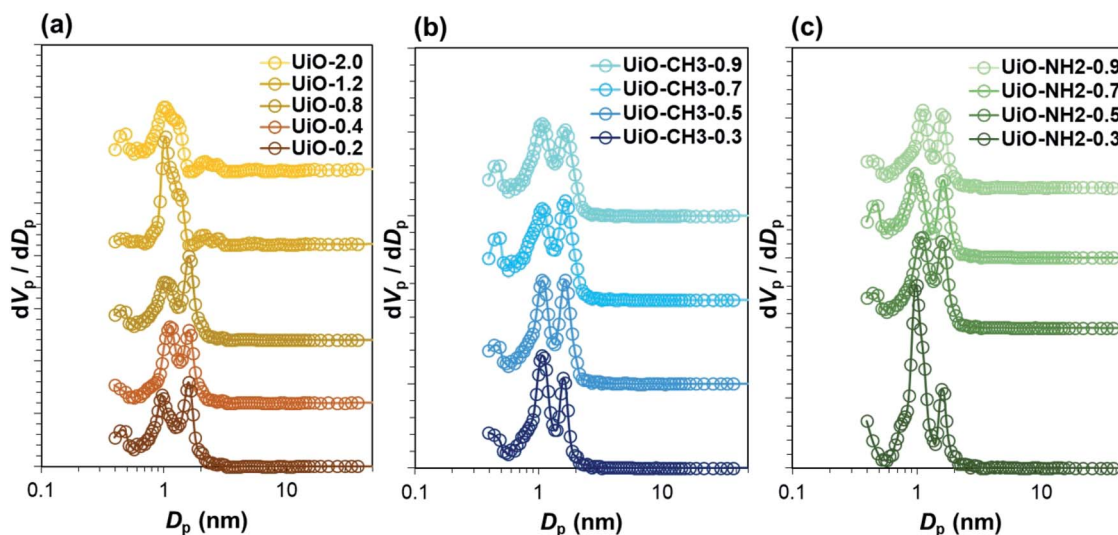


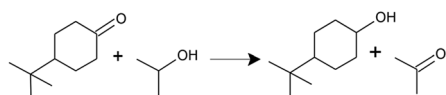
Fig. 2 Pore size distribution profiles derived by NLDFT of (a) UiO-66, (b) UiO-66-CH<sub>3</sub> and (c) UiO-66-NH<sub>2</sub> samples.

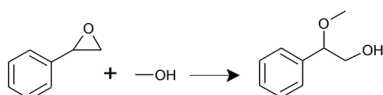


pendant coordinated-free carboxylate group as shown by the absence of C=O and COH peaks in the Fourier transform infrared spectra (Fig. S24<sup>†</sup>), suggesting a different pathway for the missing-cluster defect formation. Considering that a small amount of water hardly alters the  $pK_a$  value but greatly affects the defect formation, the origin of the missing-cluster defects is likely originated from the kinetic reason rather than the equilibrium in ligand deprotonation. On the basis of the metal cluster formation, the tetrameric species  $[Zr_4(OH)_8(H_2O)_{16}]^{8+}$  is known to be the most stable structure upon hydrolysis of  $ZrCl_4$  and  $ZrOCl_2 \cdot 8H_2O$  in aqueous solution. In the presence of carboxylate ligands, the tetranuclear species rearranges into the thermodynamically stable hexanuclear building unit with 12-ligand coordination, plausibly through the breakage of the original structure and the formation of an intermediate species.<sup>34,35</sup> At a limited accessibility to water molecules, it is anticipated that metastable species of the oxoclusters that allow a lower coordination with ligands might be formed and play a role of pre-nucleation species for the formation of the **reo** domain.

The catalytic performance of UiO-66 samples was evaluated in the Meerwein-Ponndorf-Verley (MPV) reduction of 4-*tert*-butylcyclohexanone with isopropanol (Table 1, entries 1–8) as well as in alcoholysis of styrene oxide with methanol (Table 1, entries 9–17). In the MPV reduction, UiO-66 samples were subjected to heat treatment at 150 °C under vacuum prior to the reaction. Note that the removal of the  $OH^-/H_2O$  compensating group to generate an open Lewis acidic site requires much lower temperature than that required for the removal of terminated carboxylate species<sup>11,36</sup> or dehydroxylation of a perfect framework to form a sevenfold coordinated  $[Zr_6O_6]^{12+}$  clusters with a Lewis acidic character.<sup>23,37</sup> In the blank experiment, the conversion reached 1.8% after 3 h, while it increased to 19–25% by the introduction of UiO-66. UiO-0.4, which exhibited the most intense **reo** peak, gave the highest activity among the samples. Prolonging the reaction time for UiO-0.4 to 24 h, the conversion increased up to 93.8%, surpassing those reported for missing-linker defect-type UiO-66.<sup>11</sup> The achieved conversion was in a similar range to that obtained from highly active catalysts for the MPV reduction such as Zr- and Al-beta-zeolites.<sup>38,39</sup> However, the time required to reach a similar conversion is longer for UiO-66. It is noted that the catalytic performance tended to follow the relative intensity of the (110) **reo** peak, but not exclusively. Particularly, a considerable activity was also obtained from UiO-2.0 that did not contain the **reo** domain. Instead, this sample possessed the smallest particle size and, hence, is expected to contain more under-coordinated Zr sites on the external surface. The presence of missing-cluster defects also affected the configurational isomerism of the product. The *trans/cis* ratio of the product tended to be lower for the samples containing the missing-cluster defects. It has been reported that the MPV reduction of 4-*tert*-butylcyclohexanone proceeds *via* the coordinative interaction of ketone and alcohol on a Lewis acidic site to form the cyclic six-membered transition state.<sup>39</sup> In the beta-zeolite catalyst system, thermodynamically less stable *cis*-4-*tert*-butylcyclohexanol is favored as the transition state for *cis*-isomer is less bulky

**Table 1** Catalytic performance of UiO-66 in the MPV reduction of 4-*tert*-butylcyclohexanone<sup>a</sup> and alcoholysis of styrene oxide<sup>b</sup>

				
Entry	Sample	Time (h)	Temp. (°C)	Conv. <sup>c</sup> (%)
1	Blank	3	80	1.8
2	UiO-0.2	3	80	20.9 (4.2)
3	UiO-0.4	3	80	25.6 (3.9)
4	UiO-0.4	24	80	93.8 (3.9)
5	UiO-0.8	3	80	22.8 (3.7)
6	UiO-1.2	3	80	19.6 (4.4)
7	UiO-2.0	3	80	20.9 (4.5)
8	Re-UiO-0.4 <sup>d</sup>	24	80	86.6 (3.5)

				
Entry	Sample	Time (h)	Temp. (°C)	Conv. <sup>c</sup> (%)
9	Blank	0.5	55	0
10	UiO-0.2	0.5	55	9.8
11	UiO-0.4	0.5	55	13.2
12	UiO-0.4	1	55	17.0
13	UiO-0.4	2	55	22.0
14	UiO-0.4	24	55	72.1
15	UiO-0.8	0.5	55	12.9
16	UiO-1.2	0.5	55	8.1
17	UiO-2.0	0.5	55	7.6

<sup>a</sup> 4-*tert*-Butylcyclohexanone (0.5 mmol), isopropanol (2.0 mL), a catalyst (10 mg), and *n*-decane (20  $\mu$ L) as an internal standard were heated at 80 °C. <sup>b</sup> Styrene oxide (1 mmol), methanol (1.0 mL), a catalyst (5.5 mg), and *n*-decane (20  $\mu$ L) as an internal standard were heated at 55 °C. <sup>c</sup> Determined by gas chromatography. The number in the parenthesis indicated the *trans/cis* ratio of 4-*tert*-butylcyclohexanol products.

<sup>d</sup> Nanoparticles were recovered after 24 h of the reaction and re-used after repetitive washing with methanol.

and can align along the restricted pore channels.<sup>38,39</sup> On the other hand, *trans*-alcohol becomes the main product for mesoporous catalysts.<sup>39</sup> In our case, the presence of missing-cluster defects generated the pore cavity close to mesopores. Hence, the increase in the selectivity towards *cis*-isomer is rather associated with the enhanced diffusion of the reactants to the active sites located in small pores. These results suggested that the accessibility to the active sites is rather important for the activation of bulky molecules, in which the missing-cluster defects provide not only the open Lewis sites, but also the hierarchical porous structure to facilitate the diffusion through interconnected mesopores. The catalytic recyclability and the structural retention were investigated for UiO-0.4. After 24 h of the MPV reduction, the nanoparticles were collected and re-used after repetitive washing with methanol. A slight reduction of the conversion was observed in the second run (Table 1, entry 8). The XRD patterns of UiO-0.4 after the first run and the second





run were found to be identical to the original sample (Fig. S27†), indicating that the missing cluster defects remained intact after catalysis.

In alcoholysis of styrene oxide, the as-synthesized UiO-66 samples were used without the heat treatment. The conversion reached 7–13% in the presence of UiO-66 samples after 0.5 h with 100% selectivity towards 2-methoxy-2-phenylethanol. Similar to the case of the MPV reduction, UiO-0.4 gave the highest conversion among the samples. As the Lewis acidic character of the Zr atom is shielded by  $\text{OH}^-/\text{H}_2\text{O}$  in the absence of heat treatment, it is likely that the reaction is achieved by the Brønsted acid sites *via* the addition of proton to the epoxide oxygen.<sup>40</sup> A higher activity of UiO-0.4 is believed to be associated with additional Brønsted sites at the Zr–OH/Zr–OH<sub>2</sub> defective nodes. As well, the presence of missing-cluster defects might indirectly facilitate the reaction through facile proton mobility in the hydrated environment and larger pore cavities.

## Conclusion

In summary, defect engineering in UiO-66 and its isorecticular derivatives was achieved by the rigorous control of water addition during the synthesis. Especially, we report for the first time that the missing-cluster defects can be generated without the addition of acidic modulators. This approach provides a method of fine-tuning missing-cluster defects in a simple and environmentally friendly fashion. The presence of the missing-cluster defects give rise to beneficial influences on the catalytic performance of UiO-66, where the missing-cluster defects provide additional Brønsted/Lewis acidic sites and facilitate diffusion of the reagents due to the hierarchical pore structure.

## Conflicts of interest

There are no conflicts to declare.

## Notes and references

- J. Chen, X. Zhang, F. Bi, X. Zhang, Y. Yang and Y. Wang, *J. Colloid Interface Sci.*, 2020, **571**, 275–284.
- Y. Yang, Z. Zheng, W. Ji, J. Xu and X. Zhang, *J. Hazard. Mater.*, 2020, **395**, 122686.
- Y. Wang, Y. Yang, N. Liu, Y. Wang and X. Zhang, *RSC Adv.*, 2018, **8**, 33096–33102.
- H. Li, K. Wang, Y. Sun, C. T. Lollar, J. Li and H.-C. Zhou, *Mater. Today*, 2018, **21**, 108–121.
- Y. Liu, X.-Y. Xie, C. Cheng, Z.-S. Shao and H.-S. Wang, *J. Mater. Chem. C*, 2019, **35**, 10743–10763.
- H. Wu, Y. S. Chua, V. Krungleviciute, M. Tyagi, P. Chen, T. Yildirim and W. Zhou, *J. Am. Chem. Soc.*, 2013, **135**, 10525–10532.
- W. Liang, C. J. Coghlan, F. Ragon, M. Rubio-Martinez, D. M. D'Alessandro and R. Babarao, *Dalton Trans.*, 2016, **45**, 4496–4500.
- X. Zhang, Y. Yang, L. Song, J. Chen, Y. Yang and Y. Wang, *J. Hazard. Mater.*, 2019, **365**, 597–605.
- X. Zhang, Y. Yang, X. Lv, Y. Wang, N. Liu, D. Chen and L. Cui, *J. Hazard. Mater.*, 2019, **366**, 140–150.
- X. Zhang, X. Shi, J. Chen, Y. Yang and G. Lu, *J. Environ. Chem. Eng.*, 2019, **7**, 103405.
- F. Vermoortele, B. Bueken, G. Le Bars, B. Van de Voorde, M. Vandichel, K. Houthoofd, A. Vimont, M. Daturi, M. Waroquier, V. Van Speybroeck, C. Kirschhock and D. E. De Vos, *J. Am. Chem. Soc.*, 2013, **135**, 11465–11468.
- Y. Liu, R. C. Klet, J. T. Hupp and O. Farha, *Chem. Commun.*, 2016, **52**, 7806–7809.
- D. Yang, S. O. Odoh, J. Borycz, T. C. Wang, O. K. Farha, J. T. Hupp, C. J. Cramer, L. Gagliardi and B. C. Gates, *ACS Catal.*, 2016, **6**, 235–247.
- D. Yang, C. A. Gaglioli, D. Ray, M. Babucci, L. Gagliardi and B. C. Gates, *J. Am. Chem. Soc.*, 2020, **142**, 8044–8056.
- X. Chen, Y. Lyu, Z. Wang, X. Qiao, B. C. Gates and D. Yang, *ACS Catal.*, 2020, **10**, 2906–2914.
- J. Wang, L. Liu, C. Chen, X. Dong, Q. Wang, L. Alfilfil, M. R. AlAlouni, K. Yao, J. Huang, D. Zhang and Y. Han, *J. Mater. Chem. A*, 2020, **8**, 4464–4472.
- X. Feng, J. Hajek, H. S. Jena, G. Wang, S. K. P. Veerapandian, R. Morent, N. De Geyter, K. Leyssens, A. E. J. Hoffman, V. Meynen, C. Marquez, D. E. De Vos, V. Van Speybroeck, K. Leus and P. Van Der Voort, *J. Am. Chem. Soc.*, 2020, **142**, 3174–3183.
- J. H. Cavka, S. Jakobsen, U. Olsbye, N. Guillou, C. Lamberti, S. Bordiga and K. P. Lillerud, *J. Am. Chem. Soc.*, 2008, **130**, 13850–13851.
- M. J. Katz, Z. J. Brown, Y. J. Colón, P. W. Siu, K. A. Scheidt, R. Q. Snurr, J. T. Hupp and O. K. Farha, *Chem. Commun.*, 2013, **49**, 9449–9451.
- B. Bueken, N. Van Velthoven, A. Krajnc, S. Smolders, F. Taulelle, C. Mellot-Draznieks, G. Mali, T. D. Bennett and D. De Vos, *Chem. Mater.*, 2017, **29**, 10478–10486.
- G. C. Shearer, S. Chavan, S. Bordiga, S. Svelle, U. Olsbye and K. P. Lillerud, *Chem. Mater.*, 2016, **28**, 3749–3761.
- M. J. Cliffe, W. Wan, X. Zou, P. A. Chater, A. K. Kleppe, M. G. Tucker, H. Wilhelm, N. P. Funnell, F.-X. Coudert and A. L. Goodwin, *Nat. Commun.*, 2014, **5**, 4176.
- L. Valenzano, B. Civalieri, S. Chavan, S. Bordiga, M. H. Nilsen, S. Jakobsen, K. P. Lillerud and C. Lamberti, *Chem. Mater.*, 2011, **23**, 1700–1718.
- A. W. Thornton, R. Babarao, A. Jain, F. Trouselet and F.-X. Coudert, *Dalton Trans.*, 2016, **45**, 4352–4359.
- S. Yuan, L. Zou, J.-S. Qin, J. Li, L. Huang, L. Feng, X. Wang, M. Bosch, A. Alsalmé, T. Cagin and H.-C. Zhou, *Nat. Commun.*, 2017, **8**, 15356.
- J. M. Taylor, S. Dekura, R. Ikeda and H. Kitagawa, *Chem. Mater.*, 2015, **27**, 2286–2289.
- A. Schaate, P. Roy, A. Godt, J. Lippke, F. Waltz, M. Wiebecke and P. Behrens, *Chem.–Eur. J.*, 2011, **17**, 6643–6651.
- K. L. Svane, J. K. Bristow, J. D. Gale and A. Walsh, *J. Mater. Chem. A*, 2018, **6**, 8507–8513.
- G. Y. Shangkm, P. Chammingkwan, D. X. Trinh and T. Taniike, *Membranes*, 2018, **8**, 129.



- 30 F. Ragon, P. Horcajada, H. Chevreau, Y. K. Hwang, U.-H. Lee, S. R. Miller, T. Devic, J.-S. Chang and C. Serre, *Inorg. Chem.*, 2014, **53**, 2491–2500.
- 31 F. Vermoortele, R. Ameloot, A. Vimont, C. Serre and D. De Vos, *Chem. Commun.*, 2011, **47**, 1521–1523.
- 32 B. Shan, S. M. McIntyre, M. R. Armstrong, Y. Shen and B. Mu, *Ind. Eng. Chem. Res.*, 2018, **57**, 14233–14241.
- 33 R. C. Klet, Y. Liu, T. C. Wang, J. P. Hupp and O. K. Farha, *J. Mater. Chem. A*, 2016, **4**, 1479–1485.
- 34 C. Hennig, S. Weiss, W. Kraus, J. Kretzschmar and A. C. Scheinost, *Inorg. Chem.*, 2017, **56**, 2473–2480.
- 35 M. G. Goesten, M. F. De Lange, A. I. Olivos-Suarez, A. V. Bavykina, P. Serra-Crespo, C. Krywka, F. M. Bickelhaupt, F. Kapteijn and J. Gascon, *Nat. Commun.*, 2016, **7**, 11832.
- 36 C. A. Trickett, K. J. Gagnon, S. Lee, F. Gándara, H.-B. Bürgi and O. M. Yaghi, *Angew. Chem., Int. Ed.*, 2015, **54**, 11162–11167.
- 37 M. Taddei, *Coord. Chem. Rev.*, 2017, **343**, 1–24.
- 38 J. Wang, K. Okumura, S. Jaenicke and G.-K. Chuah, *Appl. Catal., A*, 2015, **493**, 112–120.
- 39 J. C. Van der Waal, E. J. Creighton, P. J. Kunkeler, K. Tan and H. Van Bekkum, *Top. Catal.*, 1997, **4**, 261–268.
- 40 S. Ling and B. Slater, *Chem. Sci.*, 2016, **7**, 4706–4712.

